AGU PUBLICATIONS

Geophysical Research Letters

RESEARCH LETTER
10.1002/2015GL066003

Key Points:
- The 2014–2015 Fogo eruption is first event imaged with Sentinel-1 TOPS
- Eruption was fed by a single but complex dike
- Surface deformation modeling of Sentinel-1 TOPS-mode InSAR data

Supporting Information:
- Supporting Information S1

Correspondence to:
P. J. González,
p.j.gonzalez@leeds.ac.uk

Citation:
González, P. J., M. Bagnardi, A. J. Hooper, Y. Larsen, P. Marinkovic, S. V. Samsonov, and T. J. Wright (2015), The 2014–2015 eruption of Fogo volcano: Geodetic modeling of Sentinel-1 TOPS interferometry, *Geophys. Res. Lett.*, *42*, doi:10.1002/2015GL066003.

Received 4 SEP 2015
Accepted 8 OCT 2015
Accepted article online 12 OCT 2015

The 2014–2015 eruption of Fogo volcano: Geodetic modeling of Sentinel-1 TOPS interferometry

Pablo J. González[1], Marco Bagnardi[1], Andrew J. Hooper[1], Yngvar Larsen[2], Petar Marinkovic[3], Sergey V. Samsonov[4], and Tim J. Wright[1]

[1]COMET, Institute of Geophysics and Tectonics, School of Earth and Environment, University of Leeds, Leeds, UK, [2]Northern Research Institute Tromsø (Norut), Tromsø, Norway, [3]PPO.labs Laboratories for Processing Planetary Observations, Hague, Netherlands, [4]Canada Centre for Mapping and Earth Observation, Natural Resources Canada, Ottawa, Ontario, Canada

Abstract After 20 years of quiescence, Fogo volcano erupted in November 2014. The eruption produced fast-moving lava flows that traveled for several kilometers and destroyed two villages. This event represents the first episode of significant surface deformation imaged by the new European Space Agency's Sentinel-1 satellite in its standard acquisition mode, Terrain Observation by Progressive Scans (TOPS), which differs from that of previous synthetic aperture radar (SAR) missions. We perform a Bayesian inversion of Sentinel-1 TOPS SAR interferograms spanning the eruption and accurately account for variations in the TOPS line-of-sight vector when modeling displacements. Our results show that magma ascended beneath the Pico do Fogo cone and then moved laterally toward its southwestern flank, where the eruptive fissure opened. This study provides important insights into the inner workings of Fogo volcano and shows the potential of Sentinel-1 TOPS interferometry for geophysical (e.g., volcano monitoring) applications.

1. Introduction

Pico do Fogo, on Fogo Island, is the most active volcano in the Cape Verde archipelago and in the Central Atlantic oceanic region (Figure 1a), with at least 26 eruptions in the past 500 years [*Day et al.,* 1999]. After nearly 20 years of quiescence since the last eruption in 1995, a new phase of unrest started in 2014 leading to an eruption on 23 November 2014, which lasted for approximately 81 days until early February 2015. During this event, strombolian activity along a 1.2 km long radial linear fissure fed voluminous and fast-moving lava flows. On 28 November 2014, lava flows reached the village of Portela, and, by early December 2014, Portela and the neighboring village of Bangaeira had been almost completely destroyed (Figure 1b). Geodetic monitoring of Pico do Fogo volcano is routinely carried out using a permanent global positioning system (GPS) network [*Fonseca et al.,* 2003; *Fernandes et al.,* 2015]. The spatial coverage of this network is, however, not ideal to study surface displacements associated with the 2014–2015 eruption; the GPS stations are located in the far field with respect to the eruptive fissure, and they only recorded small displacements (~1 cm) (N. Pérez and B. Faria, personal communication, 2015), not providing the spatial resolution necessary to infer the geometry of the intrusive body that fed the eruption. Spaceborne radar interferometry is, therefore, the only geodetic technique that can enable us to constrain the path followed by magma in its ascent toward the surface during the 2014–2015 eruption.

Measurements of ground deformation, and in particular those from interferometric synthetic aperture radar, have proved excellent for over two decades in constraining detailed kinematic, geomechanical models of magmatic intrusions at subaerial volcanoes [*Segall*, 2010; *Pinel et al.,* 2014]. The new European Commission's Sentinel-1 mission plans to routinely acquire SAR data with an unprecedented global coverage over tectonic and volcanic areas, for an expected continuous duration of operations of 20 years [*Torres et al.,* 2012; *Elliott et al.,* 2015]. Sentinel-1A, the first of a C band dual-satellite constellation, was launched in April 2014 and reached its nominal orbit in August 2014. Sentinel-1 satellites use a new radar acquisition mode known as Terrain Observation by Progressive Scans (TOPS, see Appendix A). The onset of the Pico do Fogo eruption in November 2014 represents the first episode of significant surface deformation related to tectonic or volcanic processes to be imaged by Sentinel-1 in TOPS mode.

In this manuscript, we describe the deformation associated with the 2014–2015 Pico do Fogo eruption and highlight the potential of Sentinel-1 TOPS interferometry for studies of Earth processes associated with natural hazards (e.g., volcanic and tectonic deformation). TOPS data products are formed by merging data

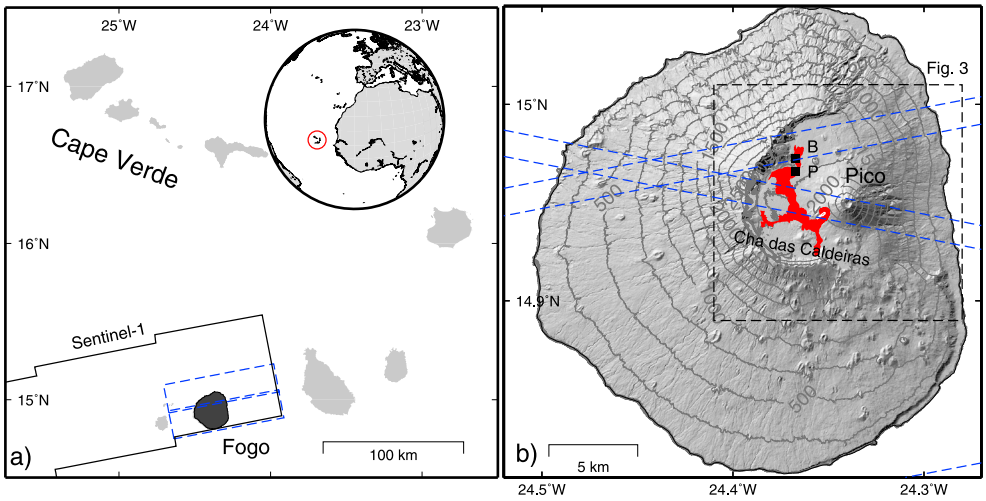

Figure 1. (a) Location of Fogo Island within the Cape Verde archipelago. For reference, we show the extent of the Sentinel-1 ascending image and the location of the two bursts that image Fogo (dashed blue polygons). Cape Verde is located off the west coast of Senegal (African continent). (b) Shaded relief map of Fogo volcano generated with bistatic TanDEM-X radar data. The 2014–2015 eruption occurred along a fissure, marked as a white line, on the lower SW flank of the Pico do Fogo and inside Cha das Caldeiras. Lava-flow extent as of 28 December 2014 is marked by the red polygon. Note the two populated areas, black squares, impacted by the eruption (P: Portela and B: Bangaeira). Dashed black rectangle shows the location of Figure 3.

subsets divided in both the across-track direction (subswaths), with variable incidence angle, and along-track direction (bursts), with variable squint angle due to steering of the satellite antenna. This results in redundancy of measurements for certain regions within each product, due to overlap between subswaths and/or bursts, and in a variable sensitivity to the along-track component of the surface displacement within each burst. In the case of the 2014–2015 eruption at Fogo, we use an overlapping region between bursts, which serendipitously coincides with the area of maximum displacement produced by the magmatic intrusion for the descending pass. The Sentinel-1 data set is compared to surface displacement maps derived using data from a higher spatial resolution C band radar satellite, RADARSAT-2. This comparison shows that the two data sets captured the coeruptive deformation equally well. We then use the interferometric synthetic aperture radar (InSAR) measurements to infer the geometry of the intrusion that fed the eruptive fissure. To accurately project modeled surface displacements into the TOPS line-of-sight (LOS) direction, we account for variability of both incidence and squint angle at each data point (Appendix A). We show that in the case of the 2014–2015 eruption at Fogo, considering a variable squint angle is of minor importance, but this may have a significant effect in the case of large displacements in the along-track direction. Our results indicate that the most recent eruption at Fogo was fed by a subvertical dike, which intruded the shallow portion of the volcanic edifice after rising from depth beneath Pico do Fogo.

2. InSAR Data

We generate ascending and descending Sentinel-1 TOPS interferograms spanning the onset and initial phases of the eruption at Pico do Fogo, using images acquired between October 2014 and December 2014. Sentinel-1 TOPS data were not acquired outside this period. To better constrain the deformation during the preeruptive and coeruptive phases and to qualitatively assess the accuracy of the Sentinel-1 data, we process additional RADARSAT-2 ultrafine mode images acquired from September 2014 to December 2014 (see supporting information). To precisely align TOPS SAR images, it is necessary to exploit the phase information from coherent pixels in the overlap regions [*Prats-Iraola et al.,* 2012], which in the case of remote oceanic islands can be challenging because only a small portion of the SAR image is over land and coherent. Nevertheless, we successfully coregister the Sentinel-1 SAR images (see Appendix A), with no visible phase discontinuities between bursts (Figures 2a and 2b).

Coeruptive Sentinel-1 TOPS interferograms show a complex surface displacement pattern localized near the eruptive fissure (Figures 2a and 2b). The ascending interferogram spanning 3 November 2014 to 27

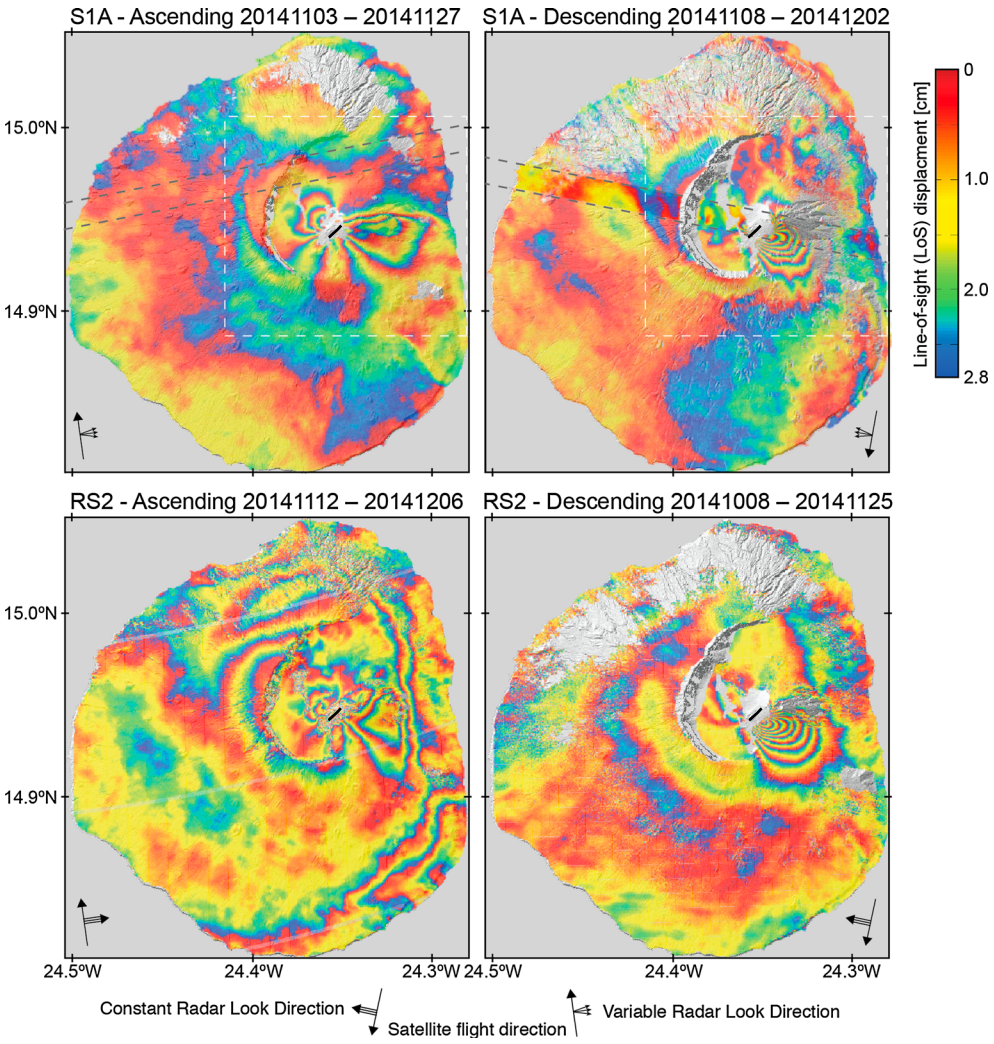

Figure 2. Interferograms of Fogo Island for the onset of the 2014–2015 Pico do Fogo eruption. (top left) Ascending coeruptive Sentinel-1A interferogram spanning 3 November 2014 to 27 November 2014; (top left) Descending coeruptive Sentinel-1A interferogram spanning 8 November 2014 to 2 December 2014; (bottom left) Ascending coeruptive RADARSAT-2 interferogram spanning 12 November 2014 to 6 December 2014; and (bottom right) Descending coeruptive RADARSAT-2 interferogram spanning 8 October 2014 to 25 November 2014.

November 2014 shows a butterfly shape with characteristics of a dike intrusion, including motion toward the satellite in areas NW and S of the fissure, and away from the satellite in the SW and E regions. The descending interferogram spanning 8 November 2014 to 2 December 2014 displays up to 25 cm of motion toward the satellite W-SW of the fissure and about one fringe of range shortening (~3 cm) NE of it. Very similar conclusions can be reached by analyzing the RADARSAT-2 interferograms (Figures 2c and 2d). The comparison demonstrates a similar accuracy in measuring phase changes between the lower resolution (~16 × 16 m pixel size averaging one sample in azimuth and five in range) Sentinel-1 data and higher-resolution (~1 × 2 m pixel size) data from stripmap mode satellite missions (e.g., RADARSAT-2). Fogo Island has been reported as a challenging location when measuring ground deformation using InSAR because of extremely variable weather conditions due to the steep topography of the volcano, which can cause water vapor delays of up to five fringes in C band interferograms [*Heleno et al.*, 2010]. For this reason, the qualitative comparison between Sentinel-1 and RADARSAT-2 interferograms becomes even more important to identify possible atmospheric contributions.

The RADARSAT-2 data set can also be used to identify deformation occurring before the onset of the eruption when Sentinel-1 acquisitions are not available. These interferograms, however, do not show any significant surface displacement prior to the eruption (supplementary information). No clear island-wide deformation is

observed in any of the interferograms spanning both preeruptive and coeruptive phases. This type of deformation would be expected in the presence of an inflating/deflating crustal magma reservoir feeding the eruption. By analyzing the temporal sequence of all available interferograms, we infer that all the observed deformation must have occurred between 12 and 25 November 2014, and most likely during a period of a few hours of intense seismicity preceding and following the eruption onset on 23 November 2014 [*Fernandes et al.,* 2015]. This deformation therefore probably reflects the propagation of the intrusion feeding the eruption and not other processes.

3. Geodetic Modeling of TOPS-Mode Interferograms

To characterize the magmatic intrusion that fed the 2014 Pico do Fogo eruption, we use a quasi-static elastic dislocation model [*Okada*, 1985] and a Bayesian inverse modeling approach. We assume that all the observed deformation occurred in a short time interval and infer the model parameters using ascending and descending interferograms from the Sentinel-1A and RADARSAT-2 satellites. We apply a Markov Chain Monte Carlo algorithm [*Mosegaard and Tarantola*, 1995; *Hooper et al.,* 2013] to estimate the multivariate posterior probability distribution for all model parameters. We assume that the measurement errors are drawn from a zero-mean Gaussian distribution. Measurements errors are considered by constructing their variance-covariance matrix. For each pair of InSAR measurements, we calculate the correlation based on a 1-D exponential covariance function: $\mathrm{Cov} = a\ \exp(-b{*}r)\ \mathrm{m}^2$, where a is the noise variance, r is the distance between the measurement points in km and b is the e-folding distance or exponential length scale—in our case, $a = 0.0016$ and $b = 0.2$. The model parameters are location, size, orientation, and uniform opening of each dike segment, a constant offset in the line-of-sight measurements for each interferogram, and a hyperparameter σ^2 (a scaling factor due to weighted misfit errors). The a posteriori distribution is sampled using a Markov Chain Monte Carlo algorithm, incorporating the Metropolis algorithm [*Mosegaard and Tarantola*, 1995]. In order to ensure fast convergence, we perform a sensitivity test for each model parameter after every 1000 iterations and adjust sampling such that all parameters contribute approximately equally to the change in likelihood and, as a whole, the mean chance of acceptance is approximately 50%. Model parameter uncertainties are presented as a posteriori probability density functions in the supporting information (Figures S7 and S8). For a full description of the method, see *Hooper et al.* [2013].

The ground motion projects differently into a TOPS variable squinted LOS direction than into a standard stripmap (constant squint) geometry (Appendix A). Therefore, to accurately project simulated displacements into the LOS direction, we consider variations in the LOS unit vector $\hat{l}$ as function not only of range, similar to stripmap images, but also of azimuth. LOS displacements are calculated as $u_{\mathrm{los}} = \underline{u} \cdot \underline{\hat{l}}$, which can be written in matrix form as

$$u_{\mathrm{los}} = -\left[u_x,\ \ u_y,\ \ u_z\right]^{\mathrm{T}}\left[(\sin\theta\cos\alpha')(\sin\theta\sin\alpha')\cos\theta\right] \tag{1}$$

where u_{los} is the TOPS LOS phase change, $[u_x, u_y, u_z]^{\mathrm{T}}$ is the transposed simulated displacement vector with east-west, north-south, and up-down components, θ is the satellite incidence angle, and $\alpha' = \alpha + \beta$, where α is the satellite heading angle, and β is the azimuth TOPS-mode burst steering angle—i.e., ±0.7° for Sentinel-1. Note that the observed motion with TOPS geometry differs from a constant squint LOS only in the contribution of the horizontal components, but not in the vertical one, as shown in equation (1).

4. Results and Discussion

We first explore the model parameters for the case of a single dike segment (model 1). The inferred location and orientation of the dike match field observations and optical imagery of the eruptive fissure remarkably well. However, large residuals (up to three fringes) are observed S and E of Pico do Fogo, indicating the need for a more complex dike geometry. Next, we test a model with two dike segments (model 2) and, without imposing any constraints on position or geometry, we find that a steeply dipping dike with similar characteristics to that in model 1 (segment A), and an additional deeper, narrow planar body beneath the NE edge of the first dike (segment B), can better explain the observed deformation. In Figure 3, we show the comparison between observed displacements, model prediction, and residuals for each interferogram. Model parameters for all optimal solutions are reported in Table S1 in the supporting information, and full a posteriori probability density functions are shown in the supporting information (Figures S7 and S8). We have also explored models allowing strike-slip and dip slip components of the motion on the dike surface, but the misfit reduction from these models was not significant enough to justify their complexity.

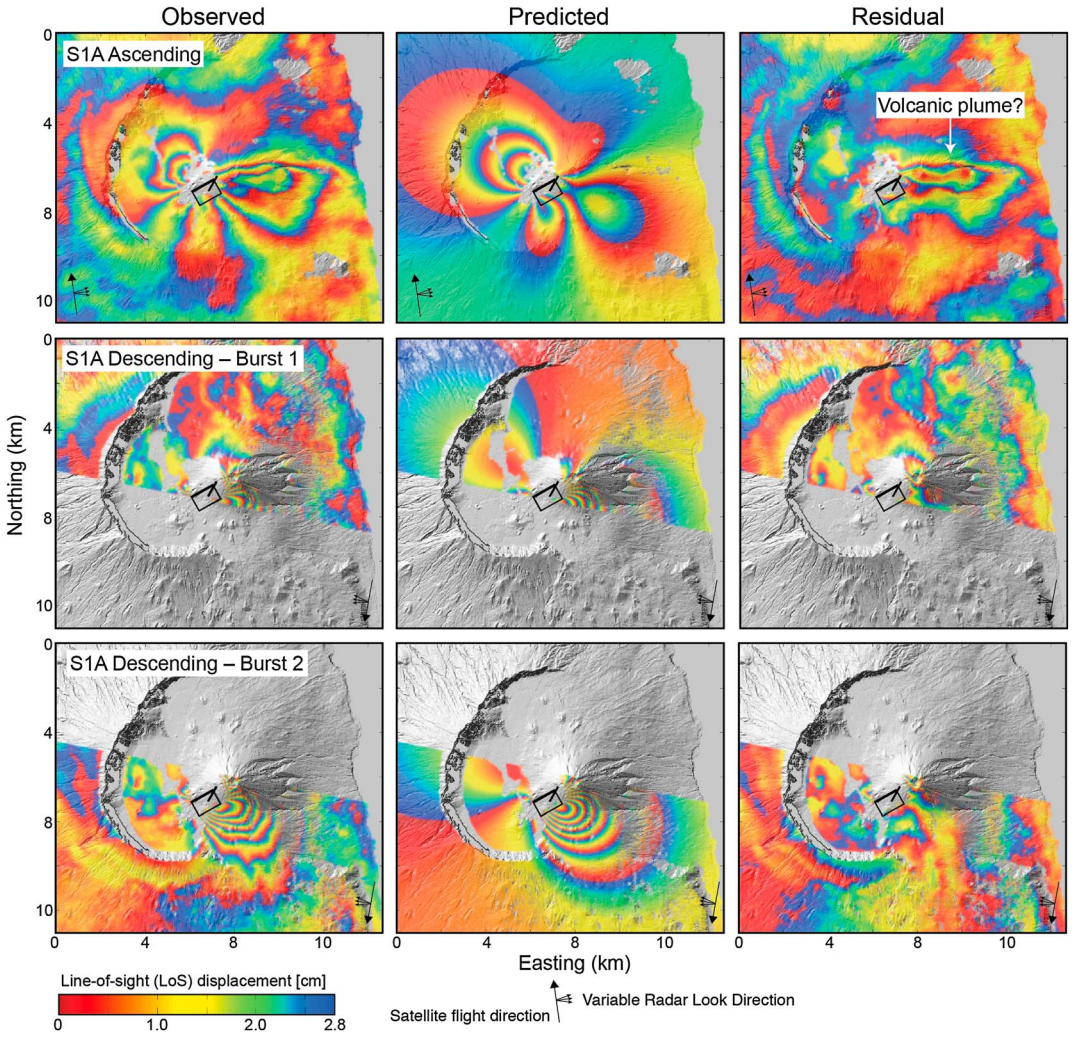

Figure 3. (left column) Sentinel-1 TOPS interferograms, (middle column) best-fitting models, and (right column) residual maps. Differential interferograms show coeruptive displacement field for the (top row) ascending 3 November 2014 to 7 November 2014 pair and the (middle and bottom rows) descending orbit for the period 8 November 2014 to 2 December 2014, separated in two bursts to highlight the use of the overlap region. The locations of the surface projection of the best-fitting tensile dislocations are marked as a black rectangle with solid lines.

A feature in the ascending Sentinel-1 interferogram that cannot be accurately reproduced by the proposed model is the interferometric phase change observed E of Pico do Fogo cone (Figure 3). We attribute this observed phase change to the presence of a water vapor-rich volcanic plume at the time of the 27 November 2014 SAR acquisition, which was used as slave image in the corresponding interferogram. This hypothesis can be supported by the analysis of Spinning Enhanced Visible and InfraRed Imager (SEVIRI) satellite visible and near-infrared images that show an eastward drifting plume on the day of the SAR acquisition (Figure S9 in the supporting information). SEVIRI data show a significant injection of volcanic material around 4 P.M. drifting in the following hours in E-SE direction (the Sentinel-1A image was acquired around 7:50 P.M.). In addition, the subsequent interferogram spanning 27 November 2014 to 9 December 2014 shows a phase-change signal of opposite sign in approximately the same area on the eastern flank of Pico do Fogo (supporting information). Therefore, we conclude that this residual phase-change cannot be attributed to a poor fit of the proposed model to the data but rather to an ephemeral source of phase change at the time of the 27 November 2014 SAR acquisition.

Our interpretation of the intrusive processes feeding the 2014–2015 Pico do Fogo eruption is consistent with previous studies of the volcano's magmatic system. *Amelung and Day* [2002] studied the 1995 Fogo eruption using European Remote Sensing InSAR data and proposed a model that includes two shallow-dike intrusions

matching the location of the 1995 eruptive fissures. The two intrusive bodies, however, counterintuitively extend in diverging directions at depth. Their proposed model may have been affected by inaccuracies in the data, due to lack of a precise digital elevation model (DEM) to remove the topographic component of the interferometric phase and large spatial and temporal baseline between SAR acquisitions. Our model for the 2014–2015 eruption implies instead the intrusion of a magmatic body that propagated from depth, first upward beneath Pico do Fogo cone (segment B, ~2.5 m opening) and then laterally (segment A, ~0.5 m opening) toward its SW flank, where the eruptive fissure opened. This model suggests that radial eruptive fissures at Fogo, the most common type of eruption in the recent eruptive history of the volcano, may be fed from subvertical radial dikes propagating from a central conduit-system rising beneath Pico do Fogo and bypass the summit of the cone. The absence of island-wide deformation during preeruptive and coeruptive phases, which was also observed in 1995 [*Amelung and Day*, 2002], further suggests the lack of crustal shallow magma reservoirs. This observation is also supported by petrological studies of the 1951 and 1995 eruptions, which suggest that the magma feeding these eruptions originated at depths greater than 15 km [*Hildner et al.,* 2011].

5. Conclusion

We successfully generate Sentinel-1 TOPS-mode interferograms free of coregistration phase artifacts and use them to constrain a mechanical model of the 2014–2015 Pico do Fogo eruption. The modeling of the TOPS LOS displacements accurately accounts for the spatially variable LOS vectors. Although the effect of considering a variable squint angle in the modeling of TOPS InSAR data may be of minor importance for the case of the 2014–2015 Pico do Fogo eruption, this should be taken into account when studying displacements of larger magnitude (e.g., earthquakes, landslides, and ice motion on glaciers) (Appendix A).

The proposed mechanical model for the 2014–2015 eruption of Fogo volcano depicts an intriguing mechanism with magma rapidly rising from depth and propagating laterally near the surface, deviating from the central conduit leading to the summit crater of the volcano. These findings could set the basis for further research aimed at understanding the pattern of eruptive fissures and underlying intrusions that have characterized the past 300 years of activity at Fogo volcano. Finally, the rapid upward migration of magmas and the lack of a shallow magma reservoir, which precludes the detection of deformation precursors to eruptions, highlight the importance of near-real-time ground deformation monitoring of Pico do Fogo volcano.

Appendix A: Sentinel-1 TOPS-Mode Interferometry

The Sentinel-1 mission was designed to obtain frequent (6–12 days) and wide-area (up to 400 km swath width) interferometric products for monitoring applications using the Terrain Observation with Progressive Scans (TOPS) mode [*Torres et al.,* 2012]. Similar to the ScanSAR acquisition mode, a TOPS image is formed by periodically switching the antenna elevation beam to points in several range subswaths (Figure A1a). The change in antenna elevation implies that only a finite number of beams per subswath can be acquired, forming a so-called burst. A Sentinel-1 image is composed of a large number of small but slightly overlapping bursts (subimages). Each burst is formed by a backward-to-forward azimuth electronic steering scan [*De Zan and Monti Guarnieri*, 2006]. Note that in the overlapping regions, data are acquired multiple times with slightly different LOS vectors, as the satellite is in different positions. The default mode of Sentinel-1 is the Interferometric Wide (IW) mode, which covers a 250 km wide swath area at 5 m (range) and 20 m (azimuth) spatial resolution.

Effectively, as a result of the antenna steering, the signal has an azimuth-varying Doppler centroid. Thus, since the phase error due to misregistration in azimuth is linear in the Doppler centroid [*Prats-Iraola et al.,* 2012], the requirements for image pairs coregistration accuracy are significantly increased. Therefore, to obtain a phase-distortion-free TOPS-mode interferogram, the azimuth misregistration error should be around 1/1000th of pixel—i.e., few centimeters for Sentinel-1. If the coregistration is not accurate, phase trends are introduced with phase jumps between bursts (Figure A1a). We implement a TOPS coregistration method based on the geometric approach of *Sansosti et al.* [2006]. Precise orbits are first used to resample a number of patches; a key aspect is that, according to the geometric model, all patches at a constant slant range have offsets with constant or very slow variation in azimuth. Thus, patch correlation functions of each slant range might be averaged/smoothed in azimuth, leading to a very precise estimate. In practice, due to the high

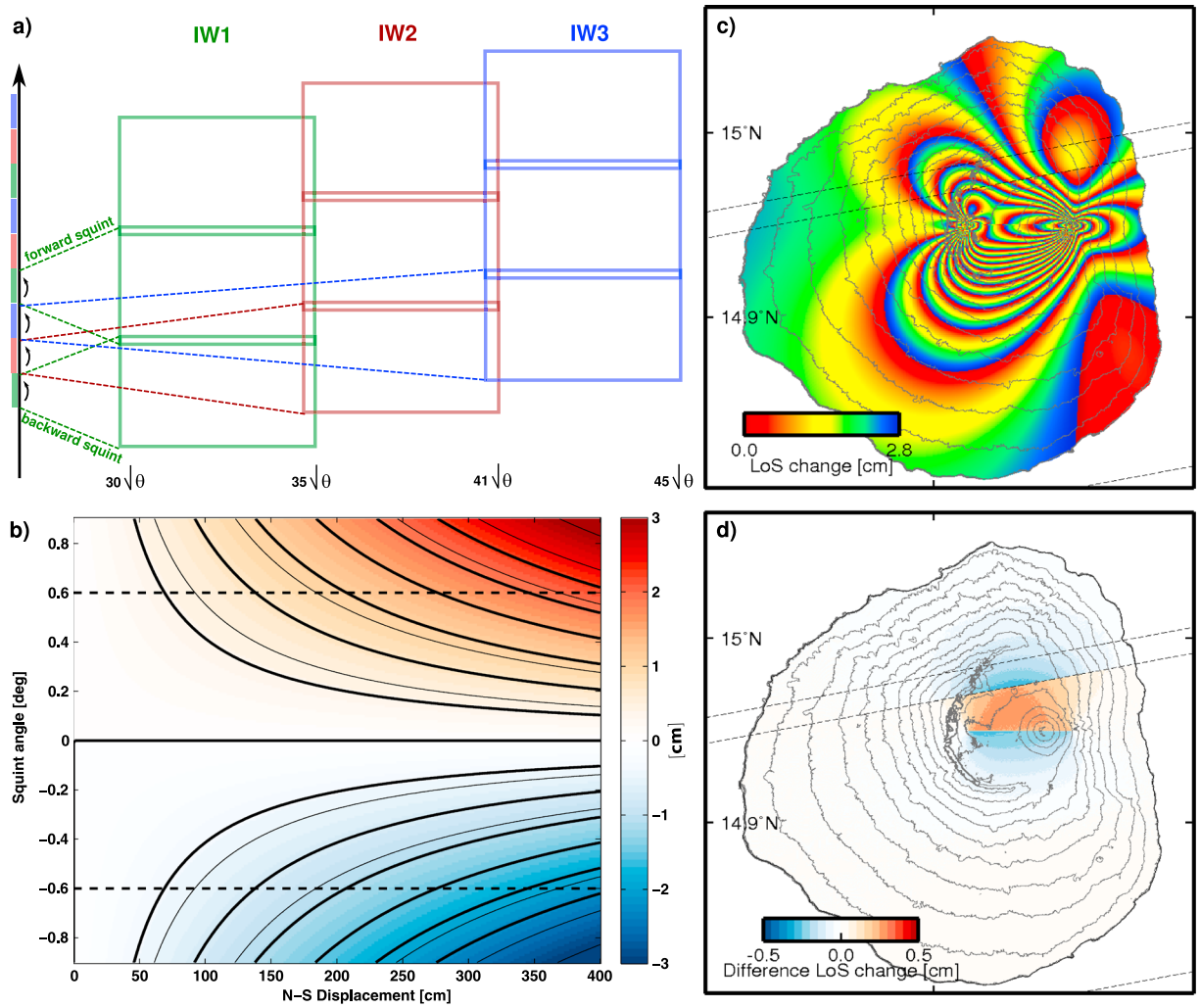

Figure A1. (a) Schematic representation of Sentinel-1 TOPS-mode IW acquisitions (three subswaths, IW1 to IW3). The TOPS radar antenna beam steers back to fore repeatedly in bursts (smaller rectangles); each burst spans ~20 km in azimuth (along-track direction). Incidence angle varies along the range distance from ~30 to ~45°. (b) Simulation of the difference in surface displacements due to the variation of squint angle (variable squinted phase contribution) as a function of north-south ground motion. Dashed lines indicate the approximate maximum value of the squint angle for the Sentinel-1 satellite. Solid lines mark contours of 0.5 cm for the far range (thick) and near range (thin). (c) Simulated ascending TOPS interferometric phase caused by the ground motion due to the intrusion of an EW oriented vertical dike intrusion (opening 1.5 m). Note the phase discontinuities at the burst edges. (d) Difference in surface displacements due to the variation of squint angle only. Note the discontinuity of ~0.4 cm at the burst overlap area, largely due to the NS component in this particular simulation.

sensitivity to azimuth coregistration errors at the burst edges, the quality of the coregistration can be quantified by utilizing the phase difference in coherent overlap areas. Any bias detected by this quality measure may be used to further refine the coregistration in azimuth. Finally, after image resampling, differential interferometry is obtained by a typical two-pass approach using an external topographic data set.

An important geophysical implication, however, arises from the required azimuth coregistration accuracy. When ground movement occurs along the azimuth direction, and the area affected by surface displacements represents a large portion of the scene, precise coregistration may fail, e.g., in ice dynamics applications. Furthermore, unlike stripmap InSAR any motion in azimuth causes LOS displacements (phase change) that are largest at the beginning and ends of the bursts due to squint angle difference. This effect should be expected to be small or negligible for most situations. In Figure A1b, we show the difference in LOS displacement due to a TOPS variable squinted LOS with respect to a stripmap constant squinted LOS vector as a function of north-south displacement magnitude using equation (1). Contour solid lines mark the 0.5 cm difference values for near-range (thin) and far-range (thick) pixels, to note a weak dependence with the

incidence angle. Dashed lines indicate the usual range of values of squint for the Sentinel-1 system. A full fringe (2π phase change, half C band wavelength ~2.8 cm) at the burst edges will be generated if the ground moves ~1.5 m in the azimuth direction. Note that the observed motion with TOPS geometry differs only on the contribution of the horizontal components, but not in the vertical one, as shown in equation (1). Differences in stripmap to TOPS LOS motion are more pronounced for the N-S component. Comparatively, LOS differences are about 4.4 times less sensitive to E-W motion. This differential ratio EW/NS shows a weak dependence on the squint angle, with a range of 4.1 to 4.7. For Sentinel-1, squint angle varies weakly for each subswath, within a range of ±0.7 (IW1) to ±0.48 (IW3). Squint angles can be calculated for each subswath as $\beta = K_\beta * (n/\mathrm{PRF})$, where n is the azimuth line number, PRF is the pulse repetition frequency, and K_β is the azimuth steering rate (deg/s), assuming zero frequency Doppler at the burst central line.

Here we simulated phase of an ascending TOPS interferogram caused by the ground motion due to the intrusion of a EW oriented vertical dike (1.5 m thickness). Note that at the burst overlapping regions the phase is discontinuous (Figure A1c). Also, note that this simulation shows a scenario in the upper range of usual magnitude of displacements observed for basaltic volcanoes [*Pinel et al.,* 2014]. In Figure A1d, we show only the phase contribution due to the squinted geometry. The changes in phase sign are the response to the relative position of the illuminated ground within each burst (squint angle) and the actual ground motion. Nevertheless, the phase discontinuity is rather small, 0.4 cm.

Acknowledgments

We would like to thank Juliet Biggs for very useful comments, and Mike Poland and anonymous reviewer for their fruitful comments. Thanks to the Sentinel-1 ESA teams, especially P. Potin, B. Rosich, J. Roeder, M. Foumelis, and Y.-L. Desnos. This research has been supported by the NERC projects: Looking inside Continent from Space (LiCS, NE/K011006/1) and Centre for the Observation and Modelling of Earthquakes, Volcanoes and Tectonics (COMET). Part of this work was funded by the ESA's SEOM programme (contract 4000110680/14/I-BG): "SEOM-Sentinel-1 InSAR performance study with TOPS data". Sentinel-1 interferograms are derived works of Copernicus data (2015). We thank the Canadian Space Agency for providing RADARSAT-2 data. Sentinel-1 radar data can be obtained from https://scihub.esa.int/dhus/. The DEM used is derived from TanDEM-X data provided through German Space Agency project XTI_GEOL0432 (https://tandemx-science.dlr.de/).

References

Amelung, F., and S. Day (2002), InSAR observations of the 1995 Fogo, Cape Verde, eruption: Implications for the effects of collapse events upon island volcanoes, *Geophys. Res. Lett.*, *29*(12), 1606, doi:10.1029/2001GL013760.

Day, S. J., S. I. N. Heleno da Silva, and J. F. B. D. Fonseca (1999), A past giant lateral collapse and present-day flank instability of Fogo, Cape Verde Islands, *J. Volcanol. Geotherm. Res.*, *94*, 191–218, doi:10.1016/S0377-0273(99)00103-1.

De Zan, F., and A. Monti Guarnieri (2006), TOPSAR: Terrain Observation by Progressive Scans, *IEEE Trans. Geosci. Remote Sens.*, *44*(9), 2352–2360, doi:10.1109/TGRS.2006.873853.

Elliott, J. R., A. Elliott, A. Hooper, Y. Larsen, P. Marinkovic, and T. J. Wright (2015), Earthquake monitoring gets boost from a new satellite, *Eos*, *96*, doi:10.1029/2015EO023967.

Fernandes, R., B. Faria, and C4G Team (2015), FOGO-2014: Monitoring the Fogo 2014 Eruption, Cape Verde, paper 12709 presented at EGU General Assembly 2015, Vienna, Austria, 12–17 April.

Fonseca, J. F., et al. (2003), Multiparameter monitoring of Fogo Island, Cape Verde, for volcanic risk mitigation, *J. Volcanol. Geotherm. Res.*, *125*(1), 39–56.

Heleno, S. I. N., C. Frischknecht, N. d'Oreye, J. N. P. Lima, B. Faria, R. Wall, and F. Kervyn (2010), Seasonal tropospheric influence on SAR interferograms near the ITCZ–the case of Fogo Volcano and Mount Cameroon, *J. Afr. Earth Sci.*, *58*(5), 833–856.

Hildner, E., A. Klügel, and F. Hauff (2011), Magma storage and ascent during the 1995 eruption of Fogo, Cape Verde Archipelago, *Contrib. Mineral. Petrol.*, *162*(4), 751–772.

Hooper, A., R. Riva, J. Pietrzak, H. Cui, G. Stelling, W. Simons, M. Naeije, E. Schrama, A. Terwisscha van Scheltinga, and A. Socquet (2013), Importance of horizontal seafloor motion on tsunami height for the 2011 M = 9.0 Tohoku-Oki earthquake, *Earth Planet. Sci. Lett.*, *361*, 469–479.

Mosegaard, K., and A. Tarantola (1995), Monte Carlo sampling of solutions to inverse problems, *J. Geophys. Res.*, *100*(B7), 12,431–12,447, doi:10.1029/94JB03097.

Okada, Y. (1985), Surface deformation due to shear and tensile faults in a half-space, *Bull. Seismol. Soc. Am.*, *75*(4), 1135–1154.

Pinel, V., M. P. Poland, and A. Hooper (2014), Volcanology: Lessons learned from synthetic aperture radar imagery, *J. Volcanol. Geotherm. Res.*, *289*, 81–113.

Prats-Iraola, P., R. Scheiber, L. Marotti, S. Wollstadt, and A. Reigber (2012), TOPS interferometry with TerraSAR-X, *IEEE Trans. Geosci. Remote Sens.*, *50*(8), 3179–3188.

Sansosti, E., P. Berardino, M. Manunta, F. Serafino, and G. Fornaro (2006), Geometrical SAR image registration, *IEEE Trans. Geosci. Remote Sens.*, *44*(10), 2861–2870, doi:10.1109/TGRS.2006.875787.

Segall, P. (2010), *Earthquake and Volcano Deformation*, Princeton Univ. Press, Princenton, N. J.

Torres, R., et al. (2012), GMES Sentinel-1 mission, *Remote Sens. Environ.*, *120*, 9–24, doi:10.1016/j.rse.2011.05.028.